Biomicrofluidics

RESEARCH ARTICLE | APRIL 03 2023

Addressable microfluidics technology for non-sacrificial analysis of biomaterial implants *in vivo*

Minh Nguyen ; Anh Tong ; Mark Volosov ; Shreya Madhavarapu ; Joseph Freeman; Roman Voronov

Biomicrofluidics 17, 024103 (2023)
https://doi.org/10.1063/5.0137932

Biomicrofluidics ARTICLE scitation.org/journal/bmf

Addressable microfluidics technology for non-sacrificial analysis of biomaterial implants *in vivo*

Cite as: Biomicrofluidics **17**, 024103 (2023); doi: 10.1063/5.0137932
Submitted: 7 December 2022 · Accepted: 6 February 2023 ·
Published Online: 3 April 2023

Minh Nguyen,[1] Anh Tong,[1] Mark Volosov,[2] Shreya Madhavarapu,[3] Joseph Freeman,[3] and Roman Voronov[1,4,a)]

AFFILIATIONS

[1]Otto H. York Department of Chemical and Materials Engineering, New Jersey Institute of Technology Newark College of Engineering, 161 Warren Street, Newark, New Jersey 07102, USA
[2]Helen and John C. Hartmann Department of Electrical and Computer Engineering, New Jersey Institute of Technology Newark College of Engineering, Suite 200 University Heights, Newark, New Jersey 07102, USA
[3]Department of Biomedical Engineering, Rutgers University, 599 Taylor Road, Piscataway, New Jersey 08854, USA
[4]Department of Biomedical Engineering, New Jersey Institute of Technology Newark College of Engineering, 323 Dr. M.L.K. Jr. Blvd., Newark, New Jersey 07103, USA

[a)]Author to whom correspondence should be addressed: rvoronov@njit.edu. **Tel.:** +1 973 642 4762; **Fax:** +1 973 596 8436

ABSTRACT

Tissue regeneration-promoting and drug-eluting biomaterials are commonly implanted into animals as a part of late-stage testing before committing to human trials required by the government. Because the trials are very expensive (e.g., they can cost over a billion U.S. dollars), it is critical for companies to have the best possible characterization of the materials' safety and efficacy before it goes into a human. However, the conventional approaches to biomaterial evaluation necessitate sacrificial analysis (i.e., euthanizing a different animal for measuring each time point and retrieving the implant for histological analysis), due to the inability to monitor how the host tissues respond to the presence of the material *in situ*. This is expensive, inaccurate, discontinuous, and unethical. In contrast, our manuscript presents a novel microfluidic platform potentially capable of performing non-disruptive fluid manipulations within the spatial constraints of an 8 mm diameter critical calvarial defect—a "gold standard" model for testing engineered bone tissue scaffolds in living animals. In particular, here, addressable microfluidic plumbing is specifically adapted for the *in vivo* implantation into a simulated rat's skull, and is integrated with a combinatorial multiplexer for a better scaling of many time points and/or biological signal measurements. The collected samples (modeled as food dyes for proof of concept) are then transported, stored, and analyzed *ex vivo*, which adds previously-unavailable ease and flexibility. Furthermore, care is taken to maintain a fluid equilibrium in the simulated animal's head during the sampling to avoid damage to the host and to the implant. Ultimately, future implantation protocols and technology improvements are envisioned toward the end of the manuscript. Although the bone tissue engineering application was chosen as a proof of concept, with further work, the technology is potentially versatile enough for other *in vivo* sampling applications. Hence, the successful outcomes of its advancement should benefit companies developing, testing, and producing vaccines and drugs by accelerating the translation of advanced cell culturing tech to the clinical market. Moreover, the nondestructive monitoring of the *in vivo* environment can lower animal experiment costs and provide data-gathering continuity superior to the conventional destructive analysis. Lastly, the reduction of sacrifices stemming from the use of this technology would make future animal experiments more ethical.

I. INTRODUCTION

Custom materials are commonly developed for implantation purposes, with some examples including engineered tissue scaffolds and drug delivery vehicles (e.g., an anti-cancer drug emitting material implanted near a tumor). Obtaining FDA approval for such implants can take 10–15 years,[1] and may cost upwards of a billion U.S. dollars.[2] Consequently, failure (which can be as high as 90%)[3] at any stage of the trials results in enormous financial losses that are often responsible for many biomedical companies going out of business or moving their operations abroad. Among the preliminary determinations, accurate forecasting of the materials' performance and safety *in vivo* are crucial to making an informed decision as to whether it makes sense to commit financial resources to the clinical

trials. Hence, animal studies constitute the last major testing step prior to performing the trials in human patients.[4] As such, they serve as the most physiologically representative predictor of the biomaterial's safety and efficacy, once it is implanted into a human.

However, the *in vivo* performance of an implanted material is notoriously difficult to analyze without explanting the sample from the animal first. In most cases, this also means euthanizing the test subject (e.g., recovering a scaffold from a cranial defect requires non-survival surgery).[5] Furthermore, the subsequent analysis is typically limited to just 2–3 signals per retrieved sample, because microscopy dyes overlap in color, and many assays are incompatible with each other. Lastly, critical spatial information, such as tissue induction (i.e., areas of vascular in-growth and cell migration from the host into the implant) and necrosis (i.e., areas of cell death due to limited nutrient supply and/or generation of excess waste products), is distorted by the explantation surgery and histology embedding/slicing.

All this balloons experimental costs and results in data discontinuity because a new animal is required for obtaining each different time point [see Fig. 1(a), where testing engineered bone is taken as an example]. Such inconsistency can lead to misleading results. Thus, the sacrificial analysis both slows down the advancement of knowledge and bottlenecks the translation of novel biomedical innovations to the clinical setting. Hence, there is a need for a technology capable of continuous monitoring within the same individual, and ideally capable of probing at separate locations within the implant nondisruptively. This would provide *continuous spatiotemporal information of unprecedented robustness* that would better inform companies regarding whether it makes sense or not to proceed with the human trials. At the end of the experiment, the scaffold could still be explanted for the end-point validation of the results. Or, the animal could be left to live out the remainder of its life with the device implanted (but disconnected from the sampling hardware). Either way, it would reduce the number of animal sacrifices required to evaluate the *initial* and *intermediate* time points [e.g., weeks 4 and 8 in Fig. 1(a)], which is more ethical [see Fig. 1(b), where only a *single* animal is required to obtain *all* time points from weeks 4 to 12 of a hypothetical experiment].

To that end, in this manuscript, we present an *implantable* version of our previously published addressable *ex vivo* microfluidics technology[6] that is capable of the minimally disruptive spatiotemporal fluid and cell sampling needed for the continuous monitoring of biomaterial implants *in vivo*. In order to demonstrate the technology's capabilities, we chose to focus on making it compatible with the critical size calvarial defect[5]—a "gold standard" model for testing engineered bone tissue scaffolds in living rats. Specifically, in this model, a round hole is created in the rodent's skull, larger than what can be healed naturally (8 mm diameter for a rat).[7] The defect is then filled with a scaffold that is intended to help the host to heal the injured bone (see the yellow disk in Fig. 2-left) better than it would have without the intervention. However, in our case, the implanted biomaterial is accompanied by a microfluidics plumbing (see Fig. 2-right).

Specifically, the idea is that once the device is implanted, the host's cells would infiltrate the implanted biomaterial that serves as the "floor" of the structure (see Fig. 2-right). Vacuum would then be applied to the microfluidics ports at the top of the device to collect microbiopsies from specific locations within the "Sampling Chambers" space, and transport the collected probings for *ex situ* analysis (thereby overcoming the need to explant the entire scaffold). The fluid samples would then be gathered on an external Sample Analysis Assay Chip (SAAC) (discussed in Sec. II C). From here, they would be analyzed by running assays in a separate microfluidics device (See Sec. III B); after which, the bone regeneration results would be recorded by a lab technician or automatically by a computer.

To that end, in this manuscript, we present a sampling technology developed for the non-sacrificial analysis of biomaterial implants *in vivo* via automated minimally disruptive manipulations of fluids in an implanted microfluidics device. For the biomaterial, we chose to work with the Poly-L-Lactic Acid (PLLA)— a synthetic polymer that is well characterized in bone regeneration studies,[8,9] However, given that this is just an alpha prototype, we first show that the idea behind its microfluidic plumbing works in a laboratory setting, with water carrying food dyes that simulate bodily fluids (as if inside of a living rodent's head), as a proof of concept. The actual implantation of the device/demonstration of its *in vivo* performance is left for a follow-up study. Furthermore, at the end of the manuscript, we offer recommendations regarding what types of assays could be potentially used for quantifying the host skull's bone in-growth into the implant based on the *in vivo* fluids collected by the device. Additionally, we refer to previously published brain microdialysis experiments[10–13] and neural cell analysis *in vivo*,[14] regarding how to better stabilize our implant and its external hardware connections on the animal's head, so that they are not torn off during use. Lastly, we offer some concluding thoughts about how to miniaturize the technology by eliminating the need for it to have connections to any external hardware.

A. Silicon wafer preparation for photolithography

4-in. silicon wafers (University Wafer, Boston, MA, Cat.# 452) were washed very carefully, before being used. The procedure involved washing the wafers with a dish soap solution (P&G, Kansas City, KS, Dawn ultra-dishwashing liquid) that has a dilution ratio of 1-to-20. Furthermore, it is important to rub and clean the wafer surface with nonwoven wipes (Texwipe, Kemersville, NC, #TX612 TechniCloth®) in a circular motion for at least 1 min and then rinse well with distilled water, using the same circular rubbing motion. Next, the wafers underwent a wet cleaning process by being submerged into an acetone bath for 10 min, at 55 °C, and then in a methanol bath for 5 min. The wafers were then removed and rinsed with de-ionized (DI) water and dried on a hotplate, at 150 °C, for 5 min (or placed into an oven, at 60 °C, overnight). Subsequently, the washed-and-dried silicon wafers were cleaned for the last time via air plasma surface treatment that lasted 30 s. Finally, the wafers were spin-coated with hexamethyldisilazane (HMDS) (Alfa Aesar, Tewksbury, MA, Cat.# 999-97-3) to enhance subsequent photoresist adhesion and dried at 150 °C, for 5 s [*Spin coating program setup*—(1) spread: at 500 rpm for 10 s with a 100 rpm/s acceleration; (2) cast: at 2000 rpm, for 30 s, with a 500 rpm/s acceleration].

B. Master mold fabrication

1. In vivo addressable microfluidic device's master molds fabrication

As shown in Fig. 3, the implanted device is designed to be composed of multiple layers, each of which requires a unique

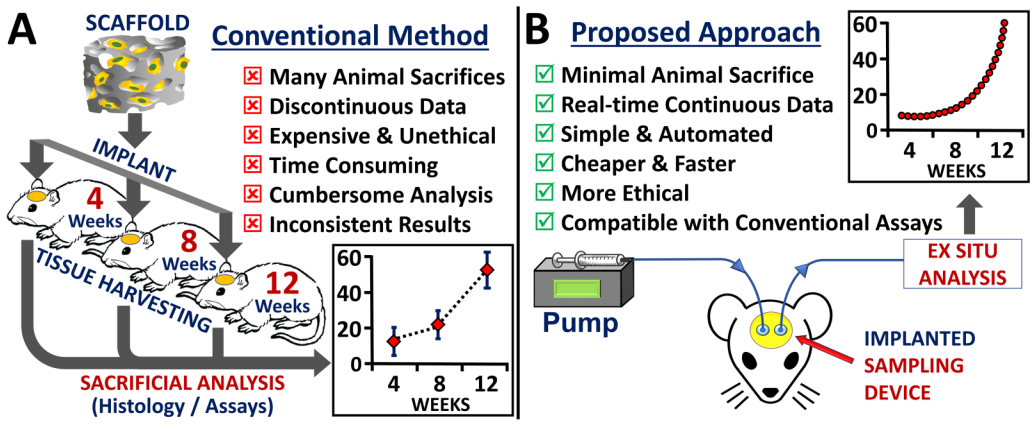

FIG. 1. Comparison of the conventional scaffold testing *in vivo* to the proposed microfluidic approach for an engineered bone evaluation example. (a) Typically, scaffolds are implanted into multiple animals, each of which is then sacrificed at various times to provide a trajectory of how the biomaterial induces bone generation *in vivo*; (b) In the envisioned approach, an implanted device continuously provides real-time cell and fluid sampling measurements of the bone formation from within the same living animal. This results in cheaper, continuous, and reliable data are obtained much faster and using less animals.

master mold: (1) control valve layer; (2) flexible membrane; (3) payload/probing plumbing layer (with addressable ports); and (4) sampling chamber layer. Initially, AutoCAD files with microscale patterns for each of the layers were printed at 50 800 dpi on 4 × 4-in. transparency films (Fineline Imaging, Colorado Springs, CO) to generate high-resolution photomasks. The procedures to create the master molds for each of the layers of the microfluidics device are described below:

a. Control valve layer. The layers were made using the same photolithography procedure: specifically, SU-8 2075 (Microchem, Westborough, MA, Cat.# Y111074 1000L1GL) photoresist was spin-coated onto wafers at 1,850 rpm, for 40 s [*Spin coating program setup*—(1) spread: at 500 rpm for 15 s, with a 150 rpm/s acceleration; (2) cast: at 1850 rpm, for 40 s, with a 200 rpm/s acceleration; (3) snap-spin to remove edge beads: at 3400 rpm, for 1 s, with a 3400 rpm/s acceleration]; expose to UV light (dose: 245 mJ/cm^2); and develop on 4-in. silicon wafers to generate 120 μm high square patterns. The developed photoresist is then fully crosslinked at 180 °C, for 2 h and then, finally, slowly cooled down to room temperature.

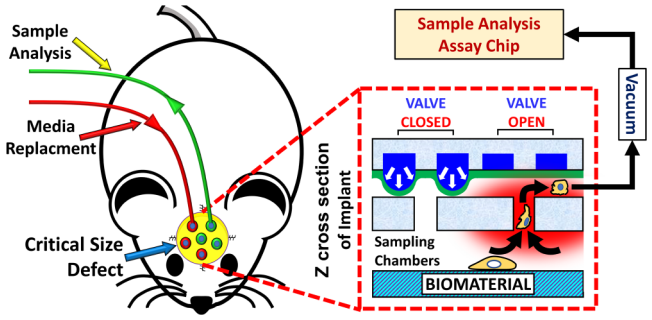

FIG. 2. Overview of the conceptualized technology. (Left) A lab rodent with a biomaterial-testing device implanted into a critical sized defect in its skull (yellow). (Right) Side view of the microfluidics device that uses the addressable ports to probe cells and fluids at targeted locations within the implant. When the blue valve is inflated, the port is closed off; but when the valve is not actuated, negative pressure is used to collect a micro- "biopsy" and send it off for *ex situ* analysis.

b. Payload/probing plumbing layer (with addressable ports). The master mold for this layer consists of *two* sub-layers [see Fig. 3(a)]: (a) round profile flow channels, created using AZ50 XT positive photoresist (EMD, Somerville, NJ, Cat.# USAW134825) and (b) addressable microfluidics ports on top of the round channels, created using SU8-2150 negative photoresist (Microchem, Westborough, MA, Cat.# Y111077 1000L1GL).

For the round profile flow channels sub-layer, the procedure was adopted from Brower *et al.* 2017 protocol.[15] Specifically, the AZ50 XT was spin-coated on silicon wafers by applying 3 ml of the photoresist to the center of the wafers and then spin-coated at 1200 rpm for 40 s to form a 55 μm ± 2 μm thickness film [*Spin coating program setup*—(1) spread: at 200 rpm, for 10 s, with a 133 rpm/s acceleration; (2) cast: at 1200 rpm, for 40 s, with a 266 rpm/s acceleration; (3) snap-spin to remove edge beads: at 3400 rpm for 1 s, with a 3400 rpm/s acceleration], followed by soft baking of the coated wafer at 110 °C on a programmable hotplate for 25 min, starting at 65 °C, and with a heating ramp rate of 300 °C/h. The wafers are then removed from the hotplate, placed in a Petri dish, and left for ambient rehydration for at least 12 h, in a dark environment. The wafers were then exposed to 930 mJ/cm^2 of UV light in 17 cycles, with a 30 s wait time in-between the exposures, and developed immediately afterward by immersing in a vessel containing 50 ml of AZ500k 1:3 developer, at 80 °C, for 8–10 min, until the round profile features emerge. At this point, the wafers are rinsed with water.

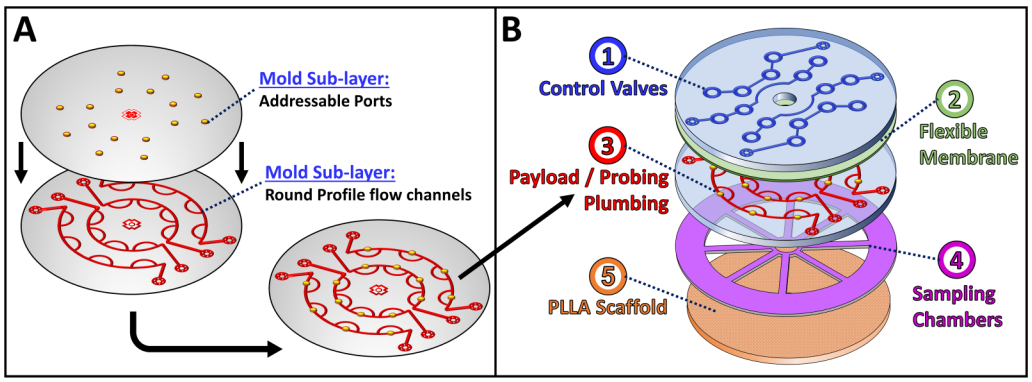

FIG. 3. Diagram showing how the payload/probing plumbing multilayered mold and the PDMS layers are stacked on top of each other. (a) The master mold for the payload/probing plumbing layer (with addressable ports) consists of two sub-layers: round profile flow channels and addressable microfluidics ports on top of the round channels. (b) The *in vivo* addressable microfluidic device is created by stacking five different 12 mm diameter PDMS layers and the 8 mm diameter PLLA scaffold on top of each other. (1) control valve layer; (2) 35 μm flexible membrane; (3) payload/probing plumbing layer (with addressable ports); (4) sampling chamber layer; and (5) 8 mm diameter PLLA scaffold.

The round profiles of the channels were created by baking the wafers at 190 °C on a programmable hotplate, for 15 h; starting at 65 °C, with a heating ramp rate of 10 °C/h.

For the addressable ports sub-layer, the SU-8 2150 was spin-coated directly onto the same wafers, at 1250 rpm, for 1 min [*Spin coating program setup*—(1) spread: at 200 rpm, for 30 s, with a 200 rpm/s acceleration; (2) cast: at 1250 rpm, for 60 s, with a 200 rpm/s acceleration; (3) snap-spin to remove edge beads: at 3400 rpm, for 1 s, with a 3400 rpm/s acceleration]; then align with the pound profile sublayer patterns using our in-house mask aligner;[16] and exposed to UV (dose: 600 mJ/cm^2). After hard baking, the wafers are then mounted on the spincoater and allowed to rotate at 100 rpm. This was followed by spraying the SU-8 developer (Microchem, Westborough, MA, Cat.# Y020100) onto the spinning wafers for 30 s-to-1 min, until the addressable port features emerged. Last, the developed photoresist was fully crosslinked at 180 °C, for 2 h, then slowly cooled down to room temperature, and, ultimately, treated with perfluorodecyltrichlorosilane (FDTS) (Alfa Aesar, Tewksbury, MA, Cat.# 78560-44-8) inside of a vacuum desiccator chamber, for 2 h.

c. Sampling chamber layer. SU-8 2150 was spin-coated directly on the same wafers, at 1150 rpm, for 1 min [*Spin coating program setup*—(1) spread: at 200 rpm, for 30 s, with a 200 rpm/s acceleration; (2) cast: at 1150 rpm, for 60 s, with a 200 rpm/s acceleration; (3) snap-spin to remove edge beads: at 3400 rpm, for 1 s, with a 3400 rpm/s acceleration]; expose to UV (dose: 600 mJ/cm^2); and immerse in a vessel containing the SU-8 developer for 30 min, to generate 600 μm-height square features. The developed photoresist was fully crosslinked at 180 °C for 2 h, and then cooled down slowly to room temperature.

2. Sample analysis chip's master mold fabrication

The sample analysis chip design consists of three layers: (1) control valve layer; (2) flexible membrane; (3) sample analysis layer (with microwells). The procedures to make the master molds for each of the layers of the sample analysis chip are similar to the described procedures for the control valve layer and the payload/probing plumbing layer (with addressable ports) in Sec. I B 1.

3. Multiplexer chip's master mold fabrication

The multiplexer chip also consists of three layers: (1) control valve layer; (2) flexible membrane; (3) multiplexed channels with junction. The procedures to make the master molds for each of the layers of the sample analysis chip are similar to the procedure for the control valve layer and the round profile flow channels sub-layer as described in Sec I B 1.

C. Microfluidic device fabrication

1. In vivo addressable microfluidic device

Different polydimethylsiloxane (PDMS) Sylgard 184 (Dow Corning Corporation, Midland, MI, Cat.# 2065622) layers of the devices were generated using soft lithography. The elastomer, with a base-to-agent ratio of 10:1, was poured over the photo-patterned control valve layer mold (from Sec I B 1) to reach a thickness of 3 mm. Then, the PDMS casted molds were degassed inside a vacuum desiccator chamber for 2 h, followed by curing on a hotplate at 65 °C, overnight (i.e., 12 h).

Flexible membrane [#2 in Fig. 3(b)] of 35 μm-thickness were created by spin-coating PDMS with a 20:1 base-to-agent ratio onto 4-in. silicon wafers at 2500 rpm, for 60 s and then baked at 65 °C for at least 1 h.

The payload/probing plumbing and the sampling chamber layers, also from Sec. I B, were created by following an established PDMS stenciling procedure.[17] Then, all of the layers were peeled off from their master molds, washed with diluted soap, submerged into an acetone bath for 10 min, at 55 °C and then, in a methanol bath for 5 min, rinsed with DI water, dried on a 180 °C hotplate, treated with air plasma and bound to each other, using our custom-

built PDMS desktop aligner,[18] to form the multi-layered microfluidic device shown in Fig. 3(b). Furthermore, during the PDMS bonding process, a biopsy punch (Electron Microscopy Sciences, PA, Cat.# 69039-05) with a diameter of 0.5 mm was used to create punch-through inlet and outlet ports for external tubing connections. The order of the single layer bonding to form the multi-layered microfluidic device was as follows: (1) control valve layer; (2) 35 μm flexible membrane; (3) payload/probing plumbing layer (with addressable ports); (4) sampling chamber layer; and (5) PLLA scaffold.

2. Sample analysis chip

PDMS with a base-to-agent ratio of 10:1 was poured over the photo-patterned control valve layer mold and sample analysis layer (with microwells) (from Sec. I B 1) to reach a thickness of 4 and 1.5 mm, respectively. Then, the PDMS casted molds were degassed inside a vacuum desiccator chamber for 2 h; followed by curing on a hotplate at 65 °C, overnight (i.e., 12 h). The process of making the flexible membrane and boding PDMS layers to form the multi-layered microfluidic device is like the procedure described in Sec. I C 1. The order of the single layer bonding to form the multi-layered microfluidic device was as follows: (1) control valve layer; (2) 35 μm flexible membrane; (3) sample analysis layer (with microwells); (4) substrate consisting of a 50 × 75 mm glass slide (Corning®, Corning, NY, Cat.# 2947-75X50) to which the device was bound to using air plasma.

3. Multiplexer chip

The process of making the Multiplexer chip is similar to the procedure described in Sec. I C 2. The order of the single layer bonding to form the multi-layered microfluidic device was as follows: (1) control valve layer; (2) 35 μm flexible Membrane; (3) multiplexed channels with junction; (4) substrate consisting of a 50 × 75 mm glass slide (Corning®, Corning, NY, Cat.# 2947-75X50) to which the device was bound to using air plasma.

D. PLLA scaffold fabrication and mineralization

The PLLA scaffolds were sketched using AutoCAD to have a donut shape with an outer diameter of 8 mm, an inner diameter of 1.5 mm, and a 1 mm thickness. They were then printed using an Ultimaker 2 + 3D printer with the following settings: 0.25 mm nozzle diameter, 0.06 mm layer height, and 80% infill. The printed PLLA scaffolds were then plasma treated for 30 s, mineralized by placing them in a 0.5M NaOH solution for 5 min, washed with DI water, and placed in an imitated concentrated bodily fluid (10× SBF) for 20 h (note: the SBF solution was changed every 2 h—to maintain a high number of ions in the solution during crystals formation/mineralization on the PLLA scaffold) and finally left in an incubator to dry.

II. RESULTS

In this manuscript, we have successfully created an alpha prototype of a novel microfluidics technology that is potentially capable of automated minimally disruptive manipulations of cells and fluids when implanted *in vivo*. These abilities are also "addressable" meaning that they can be performed independently of each other, at *any desired location* on a surface of a scaffold in an animal. To that end, this section describes the technology's ability to *collect* cellular and/or fluidic samples from within the device and transport them to an external assay chip for *ex situ* analysis (thereby overcoming the need for explantation). The nondisruptive nature of such monitoring could potentially eliminate the reliance on terminal assays; which, in turn, would drastically cheapen the cost of animal testing, ensure data continuity for multi-time point experiments and reduce the number of animals that need to be sacrificed (which is more ethical).

To that end, Fig. 4 shows a prototype of the addressable microfluidic device made from PDMS. The left-hand side of Fig. 4(a) shows the size of the device relative to a U.S. dime coin, indicating that it is small enough to fit into a critical size calvarial defect[5] in a rat's skull. The tubing on the device would be miniaturized in an actual implantation; and is, thus, omitted for clarity from the right-hand side of Fig. 4(a), which shows a zoom-in on the device's multilayered microfluidic plumbing. In addition, Fig. 4(b) shows that the microfluidics plumbing from our previously published technology[6] needs to be modified from a square grid of the addressable ports to a circularly curved one, which would fit into the implanted cylindrical device.

Furthermore, Figs. 4(c)–4(e), show a diagram and photographs of the cross-sectional view of the device, respectively. Specifically, they show that the cylindrical PDMS part of the device (i.e., the various layers and sub-layers from Sec. I C 1 that have been bonded together) is joined with the scaffold via a small bolt-and-nut. Therefore, there must be a *hole* in the center of the device through which the bolt is inserted. For example, Fig. 4(d) shows how a 0.5 cm bolt is used to connect the PDMS device and the PLLA scaffold. It should be noted that a flathead bolt is used to support the scaffold from the bottom, to minimize any protrusion into the inner space of the cranium. Furthermore, the PDMS and the PLLA parts of the device in Fig. 4(d) are intentionally separated from each other on the bolt for demonstration purposes. In contrast, Fig. 4(e) shows the two parts of the device fully pressed together with a nut on top of the bolt. This is the final configuration in which it would be implanted into the skull of an animal.

From Figs. 4(d) and 4(e), it is also apparent that the bolt was chosen to be as thin as possible (so as to minimize its interference with the microfluidic plumbing) and that its flat head at the bottom of the device is used to create a mechanical support for the PLLA scaffold. Furthermore, the latter does not add significantly to the overall thickness of the implant (given that the thickness of the rat's skull is about 1 mm). However, the bolt's presence, coupled with the space requirements of the external tubing needle connections, does add complications to the microfluidic plumbing design (which is already constrained by the small diameter of the calvarial defect that the biomaterial implant must fit into). The implications of these challenges are discussed in Sec. II A.

A. Modifying the addressable microfluidic plumbing to encircle the scaffold attachment bolt in a constrained space of the calvarial defect

As mentioned in Sec. II, the spatial constraints of the calvarial defect model,[5] coupled with its circular shape and with the need

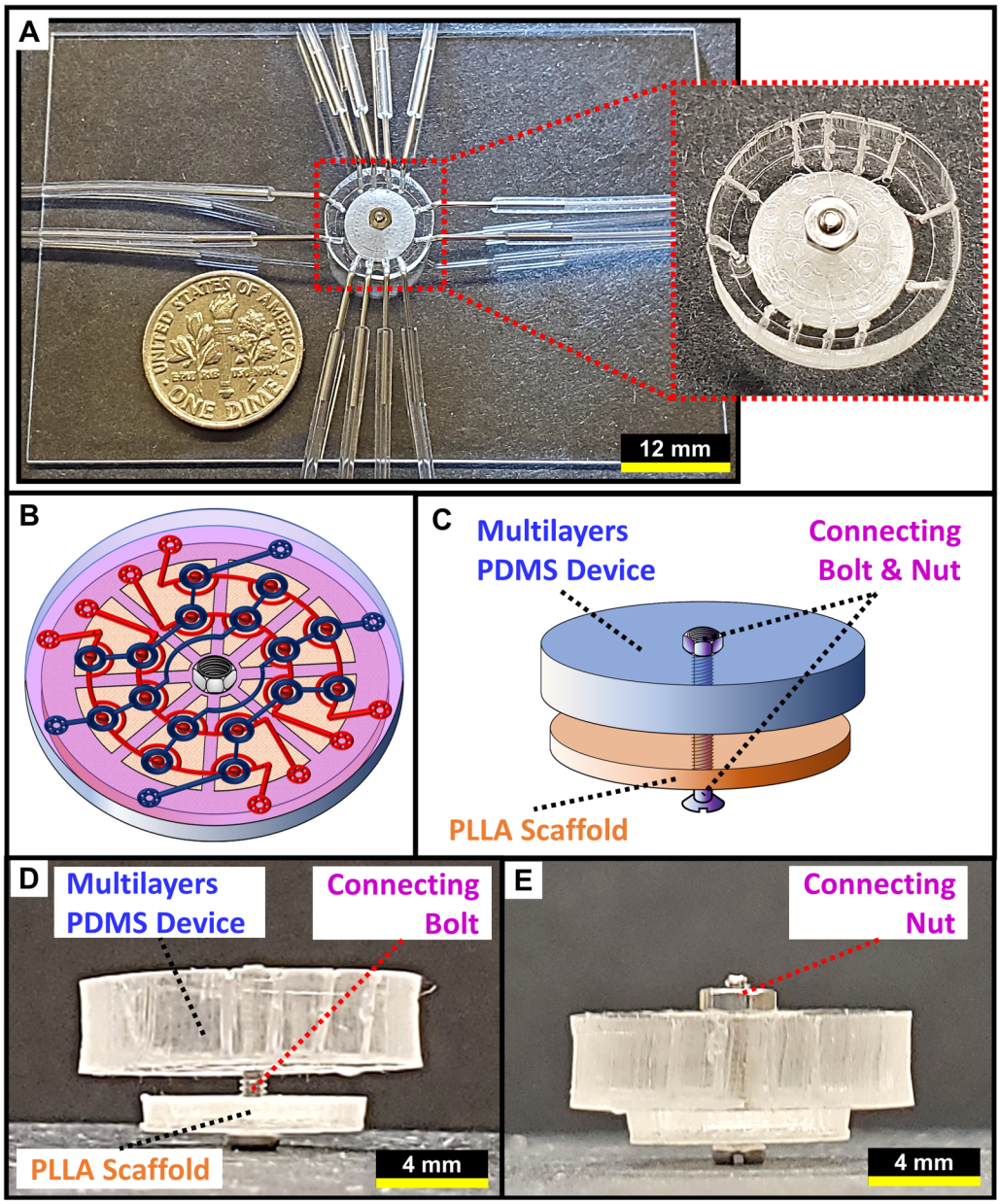

FIG. 4. Prototype of the addressable microfluidics device for non-sacrificial analysis of biomaterial implants *in vivo*. (a) The left-hand side shows a photograph of the device's size relative to a U.S. dime coin. Note that the tubing in the final implementation would be miniaturized. The right-hand side is a close-up top view of the device that has an overall diameter of 12 mm. Note that the tubing is omitted from this pane for clarity. (b) Top-view diagram of the envisioned microfluidics plumbing design, showing its circularity. (c) Side-view diagram showing how the device is joined with an 8 mm PLLA scaffold via a center bolt. (d) Photograph showing how the PDMS part of the device is joined with the 8 mm PLLA scaffold via a center bolt. Note that the two parts have not been pressed toward each other to show the beginning of an assembly. Also, the nut at the top is omitted to demonstrate a visible spacing between the PDMS and the PLLA. (e) Photograph of a stacked device, with the PDMS and the PLLA parts fully pressed against each other using the nut at the top. Please note that a flat head bolt is used in both of the latter panes to minimize protrusions into the intracranial space of the animal (see below the PLLA scaffold). View is from the side.

to have a bolt in the middle of the device (for connecting it with the biomaterial scaffold below), necessitated changes to our *original* microfluidics design that consisted of a *square* addressable ports array in our *previous* publication.[6] Therefore, in this manuscript, we have modified the addressable plumbing so that it would meet the following requirements: (1) it must fit into a limited space of 12 mm diameter (i.e., the device will be slightly wider than the 8 mm implant and will sit between the rat's skull

and the skin covering it); (2) it must curve around the center hole that fits the bolt for attaching the biomaterial scaffold below the device; (3) the various plumbing inlets and outlets must be positioned as far apart from each other as possible to allow space for the numerous tubing insertions [see Fig. 4(a)] in the constrained area of the device. If the latter are placed too close to each other, the needles that penetrate the device can create leakages between the neighboring channels and undesired stresses in the PDMS material.

Figure 5(a) shows our updated plumbing design that fits these parameters: the payload/probing plumbing layer (red) is composed of four circularly curved channels, with four addressable ports on each channel; and the control valve layer (blue), which is bonded on top, has four valves (each corresponding to an addressable port) per channel. Also, note that each of the red channels requires an inlet and an outlet (making for a total of eight tubing connections for the layer), but the blue channels only require one inlet/outlet each (i.e., four tubing connections for the Layer). Furthermore, the latter connections have been placed on the alternating sides (i.e., top-bottom-top-bottom) of the device to reduce the spatial constrainment of the needles penetrating the PDMS.

Figure 5(b) shows a PDMS prototype of the plumbing design in Fig. 5(a), using food dyes to attain the same color scheme. From this figure, it is apparent that all the channels, the inlets, and the external tubing connection needles fit snugly into the 12 mm diameter circular area of the device. Furthermore, Fig. 6 shows that the *in vivo* addressable implant is still capable of the same fluid and cell manipulation, as our original *ex vivo* addressable microfluidics device (compare to Fig. 8 and Video S1 in Ref. 6).

The action of delivering and sampling chemicals within the addressable device is shown in the left and right panes of Fig. 6, respectively. In the former case, a red dye is delivered to the top left corner of the addressable grid of microfluidic ports [see Figs. 6(a) and 6(c)], while in the latter case, the same red dye is withdrawn back via a neighboring port in the second row of the addressable matrix [see Figs. 6(b) and 6(d)]. In the *in vivo* setting, the picked-up fluids and/or cells would then be sent off to an external sensor for *ex situ* analysis on the SAAC (as in Fig. 2-right). This eliminates the need for explantation of the scaffold, ensuring continuous monitoring of the biology occurring during bone regeneration within the animal's native tissue environment. Furthermore, this can be done continuously over long periods of time, given that the entire process is automated (and as such, does not require any human involvement).

However, the actions of either delivering or withdrawing fluids within the implanted device can result in a pressure imbalance in the hosts head, which can disrupt the experiment by either breaking the biomaterial scaffold that is being analyzed and/or presenting a danger to the animal by upsetting its intracranial equilibrium. Therefore, Sec. II B presents some preventative measures in our design.

B. Maintaining cranial fluid equilibrium and preventing contamination from the surrounding tissues via sampling chambers

An additional implication of implanting a microfluidics device in the cranium of a living animal that needs to be considered is its potential interaction with the host's body, which is not desired. For example, some envisioned problems are: (1) fluid payloads delivered to the device could leak out into the host's surrounding tissues (potentially upsetting the intracranial fluid pressure in the animal's head and potentially hurting or even killing it); (2) a reverse situation could occur where a mix of the host's bodily fluid/cells from the areas surrounding the implant could contaminate the probings collected from the sampling chambers of the device; and (3) if excess vacuum or pressure are created in the device, they could cause the scaffold to collapse or break (thereby jeopardizing the experiment and endangering the animal's well-being). Therefore, it is desirable to: (a) isolate the microfluidics portion of the device from the host's physiology and (b) maintain a fluid equilibrium inside of its chambers such that no excess pressure or vacuum is created by the performed plumbing manipulations. In other words, if any fluid is flown into the device, an equal amount must be removed from it somewhere else simultaneously (and vice versa).

To take care of these issues, we have included a sampling chamber layer, situated between the PDMS part of the device and the biomaterial scaffold [see Layer #4 in Fig. 3(b), and also see Fig. 7(a)]. It serves two purposes: (1) the thick circular band, along the circumference of the layer, serves as a "wall" that sits on top of the skull bone (attached with fibrin glue) and isolates the device's microfluidic plumbing from the interstitial fluids of the host's body [see purple color in Fig. 7(a)]; and (2) the area inside of the circle is broken up into eight identical "pizza slice"-shaped chambers [see Fig. 7(b)], which effectively divide the surface of the implanted scaffold into separate sampling regions (green color). The reason why this is important is because it: (a) reduces diffusion between the neighboring regions, thereby increasing the spatial accuracy (i.e., "resolution") of the probing; and (b) isolates two addressable microfluidic ports per each "pizza slice"-shaped chamber [see Fig. 7(c)]. The latter is a fluid pressure balancing measure: essentially, while one port is active (i.e., delivering or sampling fluid), the other port in the chamber is kept open to prevent any pressure or vacuum build-up that could potentially lead to the collapsing of the PDMS device; or to the deformation/cracking of the PLLA scaffold and/or causing brain damage in the mouse, due to the strong pressure/vacuum forces transmitted through the PLLA's pores. For example, when one port is open to a vacuum line to collect a sample, the neighboring port would be open to a fresh media source to quench the negative pressure in the same chamber [see Figs. 7(a) and 7(c)].

Ultimately, as the probings are collected, they are sent off to a SAAC, which is discussed in the section.

C. Storing and analyzing collected *in vivo* samples on an *ex vivo* assay chip

As mentioned in Sec. II B, as the probings are collected within the microfluidic implant, the pressure balance within it will need to be maintained. For this reason, the implant will be connected to a media replacement storage (see Fig. 8-left), which will provide the fluids necessary to substitute the volumes subtracted by the probings. In other words, the microfluidic device will draw the replenishment media from this storage as it is collecting samples from the "pizza slice"-shaped sampling chambers (see Fig. 8-center), to

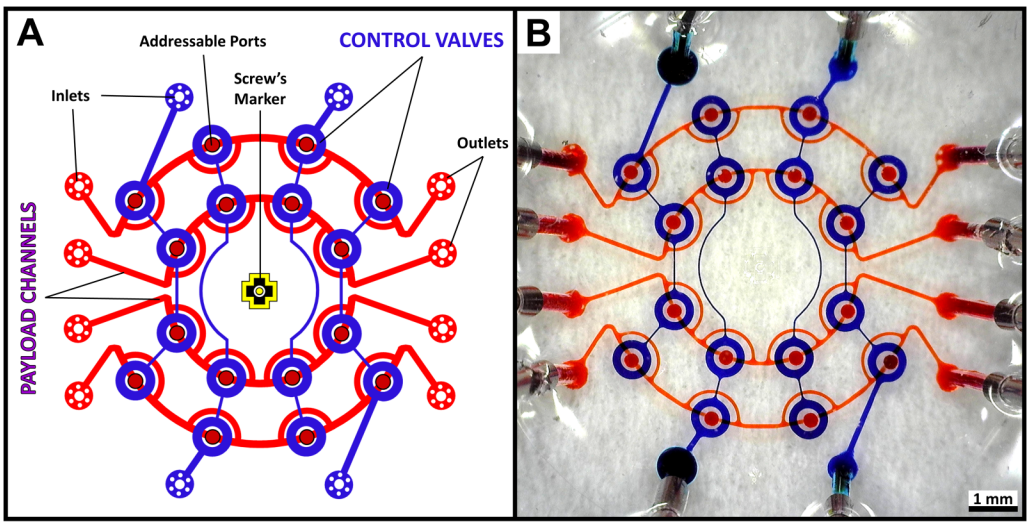

FIG. 5. Novel design of the circularly curved addressable microfluidic plumbing intended for the *in vivo* implantation: (a) Top-view schematic of the control valves (blue) and the payload/probing plumbing (red) layers, aligned on top of each other. The yellow-and-black cross is an alignment mark, which also designates the placement of the screw that attaches the biomaterial scaffold below the device. (b) Microscopy image of the fabricated microfluidic design in pane A. Channels and valves are highlighted using food dyes to achieve the same color representation. View is from the top of the device.

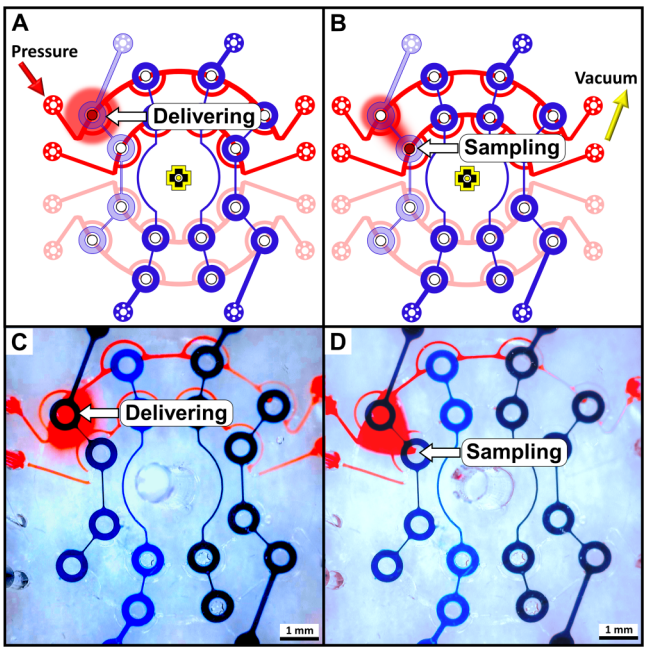

FIG. 6. Addressable fluid manipulation demo in the implantable device: (a) diagram of delivery of a red dye to the top left corner port in the first/top curved address row; (b) diagram of sampling of the delivered red dye via a neighboring port in the second curved address row. The yellow/black cross is an alignment mark that also shows where the bolt will go through. (c) and (d) are microscopy equivalents of panes (a) and (b) in the fabricated device, respectively. The view is from the top of the device.

maintain the net amount of fluid in the device constant. Once the probings are obtained, they will be flowed out of the implant and into the *ex vivo* SAAC (see Fig. 8-right), thereby overcoming the need for sample explantation.

When on the chip, the collected probings can be either stored to be subsequently removed by an operator for off-line analysis; or on-chip assays can be performed directly in the storage wells. For the latter option, some potential chemical tests that are appropriate for the calvarial defect bone tissue engineering application are discussed in Sec. III B, while this part of the manuscript is limited to the design of the chip.

The chip's plumbing is basically a microfluidic analog of a conventional well plate (e.g., 96 well plate), with each of the storage compartments being individually addressable (see Fig. 9). It has been previously published[17,19] and requires no modifications, aside from selecting an appropriate number of rows and columns for the well matrix: given that the dimensions of the chip are not limited by the *in vivo* size constraints, it is important to note here that the chip can be basically made to be *any* size, because as many (or as few) probings as needed can be processed by it at *any* desired frequency. However, here, we have designed it with *four* rows of wells to match the number of payload/probing plumbing channel rows in Fig. 5/6, because this reduces the plumbing complexity. Meanwhile, the chip's number of columns remains a free parameter, which would be determined based on the number of the desired timepoints, locations and/or signals that the user wants to measure. This is shown in Fig. 9-right.

For example, a *single* time point measurement at all 16 addressable port locations in the implant would require four columns (i.e., a 4×4 matrix of wells), while storing *two* timepoints would require *eight* columns (i.e., a 4×8 matrix of wells), and so

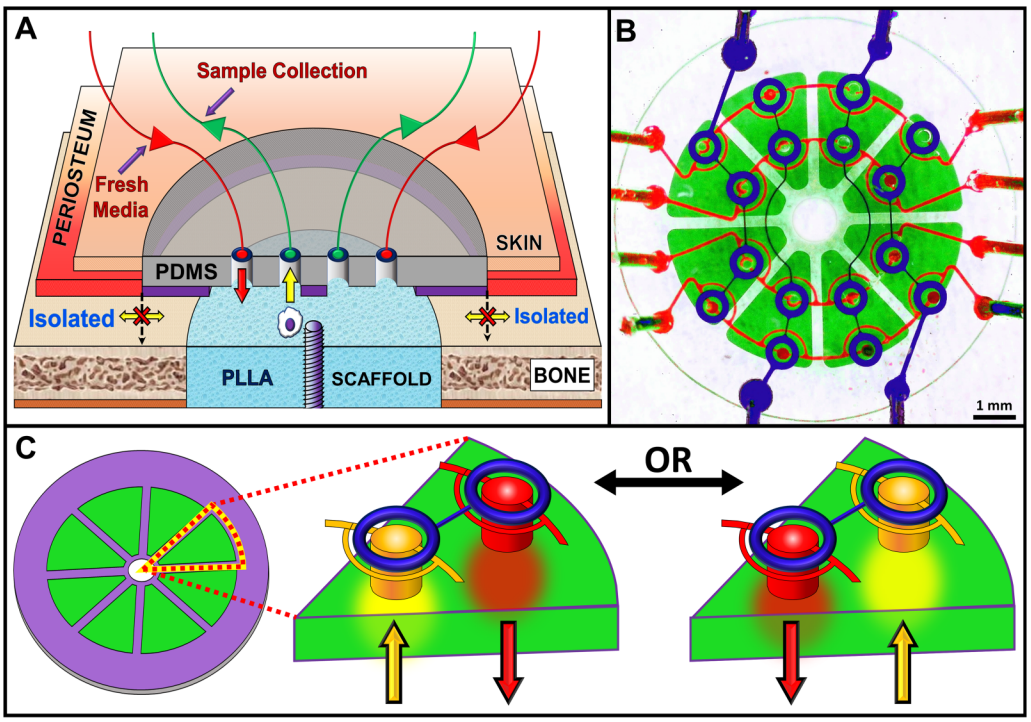

FIG. 7. Isolation of the addressable microfluidic implant from the host's tissues and pressure rebalancing via the sampling chamber layer. (a) Diagram explaining how the device's various layers are leveled when implanted *in vivo*. The sampling chamber layer (purple) is between the PDMS (clear) and the scaffold (cyan). Since the former is wider than the latter, the layer's outer edge sits directly on top of the animal's skull and blocks any fluid and/or cell transport in the radial directions. Also shown is the fluid replenishment (red arrows) that occurs in tandem with the sampling (yellow arrows) to maintain a pressure balance. The screw is omitted for clarity. (b) Microscopy image that uses food dyes to highlight the device's "pizza slice"-shaped chambers (green), control valves (blue), and the payload/probing plumbing (red). View is from the top. (c) (Left) Diagram of the sampling chamber layer showing its walls in purple and the void space from which the probings can be taken in green; (center/right) a zoom-in of a "pizza slice"-shaped chamber that shows two addressable ports working in tandem to quench any positive or negative pressure excess build-up: when one port is probing samples (yellow), the other one is open for the media replenishment to flow in (red), and vice versa.

on. Alternatively, if an entire "pizza slice"-shaped sampling chamber is considered to be a *single* "location" [since the addressable ports work in tandem pairs, as was shown in Fig. 7(c)], then the number of the wells per timepoint would be *halved* (i.e., 2 chamber rows × 4 chamber columns → a total of 8 storage wells would be required). *Conversely*, if one wanted to measure *multiple* biological signals per timepoint at each location, then the number of the total wells from the examples above would be multiplied by,

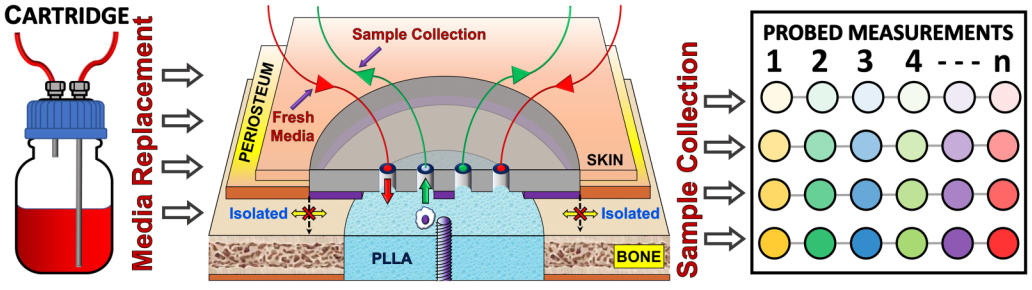

FIG. 8. Diagram of the implanted biomaterial-testing device's operation. (Left) Storage bottle from which the fresh culture media and maintenance drugs are replenished; (center) diagram showing the microfluidic device receiving the replenishment media from the storage, as it is sampling the *in vivo* environment above the PLLA scaffold implant and sending off the results to the SAAC; (right) diagram of a possible iteration of the SAAC, in which its matrix of wells consists of four rows (to match the four rows of payload/probing plumbing channels in Fig. 5/6); and the number of columns in the matrix remains a free parameter (that would be determined based on the number of the desired time points, locations and signals that the user wants to measure).

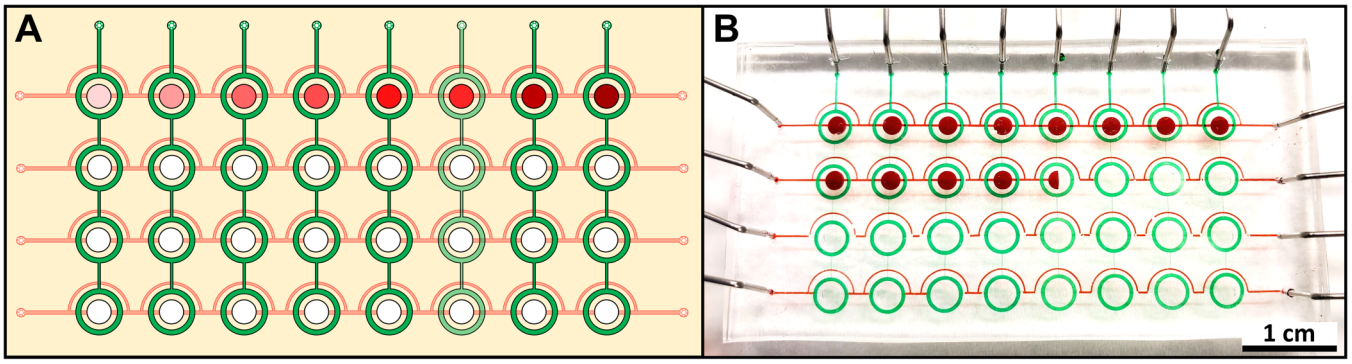

FIG. 9. A prototype of the Sample Analysis Assay Chip (SAAC). (a) Diagram of a 4 × 8 array of addressable microfluidics sample analysis wells. (b) Microscopy image of a fabricated 4 × 8 sample analysis chip. Food dyes are used to highlight the addressable circular valves (green) and the sample payload channels and storage wells (both red). The latter are shown at different stages of being filled (i.e., fully, partially, or not at all). Each well has a 20 μl volume. The view is from the top.

however, many signals are being detected. For example, in Sec. III B, we propose to measure *four* different biological signals per a sampling chamber. This would translate to a chip with a total of 32 wells. So, for demonstration purposes, we have designed a SAAC with a 4×8 addressable grid of storage wells [see Fig. 9(a)]. Fig. 9(b) shows a working prototype of the envisioned array of the micro-wells.

In Sec. II D, we discuss how the external hardware requirement (which is ultimately related to system price and experiment setup difficulty) scales with the increasing SAAC size as well as how to reduce that requirement at a "cost" of an additional microfluidic plumbing complexity.

D. Reducing the external equipment requirement via a combinatorial multiplexer chip

Given that the addressable microfluidic plumbing requires a considerable amount of external hardware equipment (e.g., pneumatic solenoid valves, pressure regulators, gauges, etc.)[20] to run, managing two such chips (i.e., the addressable implant and the SAAC) can become costly and complicated. Furthermore, if many locations, timepoints and/or biological signals need to be measured between the SAAC replacements, then the growing size of the latter will increase that requirement even further. To put it into perspective, the 4×4 implantable device described in Sec. II A uses a manifold of eight solenoids (costs ~ $600)— the costliest components in the system—to actuate its four control valve channels and four flow channels.

Moreover, the cost accumulates further for the hardware needed to run the SAAC: although its rows can be run by the same solenoids as those actuating the implant's payload/probing plumbing channels (because they are basically shared between the two chips), its columns do require extra solenoids to operate. That is, for each additional eight well columns, the cost goes up another $600. So, for a typical 3-day experiment, with a 4-hour probing frequency (i.e., 6 times per day), the number of the columns in the SAAC that detects four biological signals per implant (as in Fig. 9) would have to be increased from 8 to $3 \times 6 \times 8 = 144$. That is, the solenoid cost of running a SAAC of this size would go up by a factor of 18 (which translates to an equipment cost >$10 000 and to an unnecessary tubing/wiring complexity).

Luckily, a *Combinatorial Multiplexer* concept in microfluidics offers a way to reduce the external hardware requirements (albeit at a penalty of increasing the complexity of the on-chip's plumbing).[21] In particular, due to its $N!/(N/2)!^2$ scaling, up to 252 lines can be actuated with just 10 control lines (i.e., with only 10 solenoids). This means that by simply adding the multiplexer to our flow system, the equipment cost of running the 144 column SAAC in the example above can be reduced by a factor of 10. Thus, it is worthwhile to include the combinatorial multiplexer into our design, to make the system costs and setup be more manageable.

To that end, Fig. 10 shows our integrated system, with all three of the microfluidics chips connected: the addressable implant, the SAAC and the combinatorial multiplexer. For the latter, we have opted to use the 8 control lines version [multiplexer rows in Fig. 10(a) corresponding to yellow tubing in Fig. 10(b)], since it can actuate up to a total 70 flow lines [multiplexer columns prior to Junctions in Fig. 10(a)], while our system described in Fig. 7(b) and in Fig. 9 requires less than that to run. In fact, multiplexing just 40 flow lines is sufficient for operating the addressable implant and the SAAC described in Secs. II A and II C, respectively. Therefore, the remaining 30 unused flow lines of the multiplexer are not fabricated (and are, thus, not shown in Fig. 10).

As far as the 40 flow lines that are used, they are *merged into pairs* [see the 20 numbered *Junctions* in Fig. 10(a)]. For example, the red Junctions #1–4 are dedicated for multiplexing the inputs of the payload/probing plumbing on the addressable implant. Each of the junctions allows the system to alternate between two different fluid and/or pressure source inputs, while combining them into a single multiplexed output. For example, one of the two lines belonging to the Junction #1 is shown to be *active* (bright red), while the other is *not* (dim red). The multiplexer can alternate between them to flow fluids containing different drugs, media, etc., through the payload channel resulting from Junction #1. Likewise, it can also alternate between *pressurized* and *non-pressurized* blue lines that belong to control valve Junctions #5–8, to either inflate or deflate the blue O-shaped valves on the addressable implant.

Similarly, the green Junctions #9–16 in Fig. 10 are used to either inflate or deflate the addressable O-shaped valves on the SAAC. Last, the red Junctions #17–20 in the same figure are used in tandem with the first four junctions to flow the payloads/samples through the four rows in the addressable implant and SAACs. However, in the case of the former junctions, the multiplexer alternates between *non-pressurized* and *vacuum* lines. The negative pressure, in turn, helps to pull the payloads and/or samples through the two chips.

An example of the multiplexer's operation is also shown in Fig. 10(a): by actuating its control lines #4 and 6–8, the multiplexer allows for flow to only go through the *right* arm of the red multiplexed Junction #1, while the rest of the junctions are fully blocked. Similarly, it can activate or disable the inflatable O-shaped valves on the addressable implant and the SAAC to achieve the addressable manipulation at the targeted microfluidics ports or wells, respectively. To that end, Fig. 10(b) shows an actual system prototype using the multiplexer to fill the top row of the SAAC with a red dye.

Next, Table I shows how the choice of a different-sized multiplexer affects the total number of time points and/or biological signals (see the last column in Table I) that can be stored/analyzed on the SAAC. For these calculations, we assume that the implantable device's matrix of addressable ports remains at the fixed size of 4×4 presented in this manuscript, which takes eight payload/sampling lines [red arms of the Junctions #1–4 in Fig. 10(a)], eight control valve lines [i.e., blue arms of the Junctions #5–8 in Fig. 10(a)] to operate, and eight vacuum lines to operate [i.e., red arms of the Junctions #17–20 in Fig. 10(a)].

To explain how Table I is calculated, we provide an example for its first row. Here, we are examining an 8-control line version of the combinatorial multiplexer. Its theoretical maximum is the actuation of 70 flow lines, as per the formula: $N!/(N/2)!$,[2] where $N = 8$. Out of these 70 flow lines, 24 must be dedicated to operating the addressable implant chip. So:

70 (total possible multiplexed flow lines) – 8 (implant payload channels) – 8 (implant control channels) – 8 (sample chip vacuum channels) = 46 (remaining possible multiplexed channels).

Next, we must account for the fact that takes *two* flow lines to operate a *single* addressable microwell column on the SAAC, because pressures and non-pressurized lines must be merged together into a single control valve channel (see the formation of green Junctions #9–16 in Fig. 10). Therefore, the number of total possible addressable microwell columns on the SAAC is equal to half of the remaining possible multiplexed channels:

46 (remaining possible multiplexed channels)/2 (multiplexed channels per junction) = 23 (remaining possible multiplexed junctions) → 23 (total possible microwell columns).

Next, we must translate the number of columns on the SAAC translates to the number of microwells. Staying with the assumption that the addressable implant chip has four payload/sample flow channel rows, this means that the number of SAAC wells is quadruple of its columns (because the row channels are shared between the two chips):

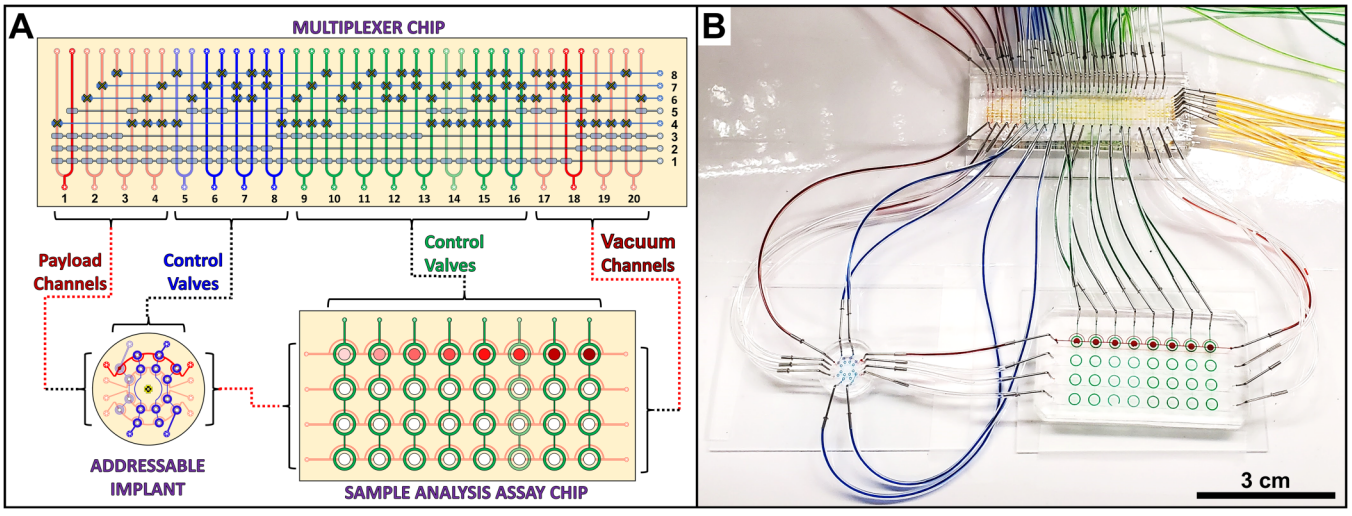

FIG. 10. A prototype of the overall plumbing setup for the addressable microfluidic implant and the two chips supporting it. (a) Diagram showing the plumbing setup—all three microfluidic systems working together in unison: the combinatorial multiplexer actuating the addressable implant and the SAAC. Junctions #1–4 of the chip are dedicated for the inputs of the payload/probing plumbing on the addressable implant; Junctions #5–8 are dedicated for the control valves on the same chip. Junctions #9–16 actuate the control valves on the SAAC; and then the output of the SAAC is actuated with negative pressure from Junctions #17–20. Control lines #4 and 6–8 of the multiplexer are actively blocking all lines, except for the right arm of Junction #1 (red). This enables flow through the top row (red) of the addressable implant. (b) Microscopy image of a fabricated system prototype with food color highlights. The implantable device is in a dish. Note: Although a combinatorial multiplexer consisting of eight control lines (yellow) can operate up to 70 flow lines (red, green, and blue), we are only showing the portion that is needed to run the system.

*4 (implant channel rows) * 23 (total possible microwell columns) = 92 (total possible SAAC microwells).*

Last, assuming that the user wants to store/analyze every location in the 4 × 4 addressable matrix, each time point or biological signal measured would have to consume 16 (or 8, if each sampling chamber is treated as a "location") SAAC microwells:

92 (total possible SAAC Microwells)/16 (implant probing locations) = 5.75 (time points and/or signals).

Given that the final answer is not a whole number, we round it down to the nearest integer to get that 5 (or 11, if each sampling chamber is treated as a "location") total timepoints and/or biological signals that could be stored/analyzed on the SAAC.

III. DISCUSSION AND FUTURE WORK

In this manuscript, we have developed a microfluidics technology potentially capable of testing biomaterial implants *in vivo*, thereby bypassing the need for conventional explantation analysis (which is tedious, expensive, and requires a lot of animal sacrifices). Specifically, the novel design is based on a previously published addressable *ex vivo* microfluidics technology,[6] but with the following key differences: the original device was made to be a *rectangular* 50 × 75 mm chip so that it could be mounted on a microscope stage (see Fig. 4 in Ref. 6). In contrast, the *in vivo* version has been miniaturized so that it could fit into the round 8 mm diameter hole of the calvarial defect in the animal's skull. Furthermore, because this constraint also requires the device to be *circular*, its plumbing design has been modified to account for the roundness and to accommodate the screw hole (which is needed to attach the studied biomaterial scaffolds) in its center. Last, the implantable device had to be coupled with the external sample storage chip and the multiplexer, which was not the case with the original stand-alone device.

The successful accomplishment of these modifications, and the subsequent testing with food dyes, has made us confident that our device should be able to accomplish the envisioned sampling of the cell secretions occurring in the host's body nondisruptively and then transporting the collected fluids *ex vivo* for subsequent analysis (which is significantly cheaper and easier than the status quo). However, further work needs to be done to demonstrate its efficacy in a non-simulated environment (i.e., sampling real bodily fluids instead of the food dyes).

Additionally, the fluid manipulation repeatability needs to be further tested over many cycles. Having said that, the repeatability of the on-chip fluid manipulation depends on several factors:

(1) The shape and dimensions of the valves—even though the valves in this manuscript have a different spatial arrangement from the original design in Ref. 6, we have retained their same shape and dimensions from the previous work. Therefore, their repeatability should be the same as was shown in an unmonitored operation regime in our previous publication (see Video S1 in Ref. 6).
(2) The thickness of the PDMS membranes that block/unblock the flow—the PDMS is typically chosen for the microfluidics valve material because of its durability, elasticity, and non-degradability. Work by other researchers showed that similar valves can undergo as many as 65 h with 585 actuations.[22] However, our 35 μm-thick membrane is significantly *thinner* than the 200 μm-thick one tested in the above study. Therefore, our PDMS membrane should be more flexible/elastic and, thus, is expected to be more durable.
(3) The operating pressure that inflates the on-chip valves—previous work by others has shown that the main cause of valve failure is high pressure. Specifically, it was mentioned that the normal microfluidic operating range is 0.138–0.310 MPa (20–45 psi).[23] In contrast, our device uses 20 psi, which is the lower edge of the limit (meaning that the air pressure should not be damaging it).
(4) The macroscopic external electronic solenoids that actuate the microscopic on-chip valves—these are rated for millions of cycles and are, therefore, not expected to be a significant contributor to the fluid manipulation repeatability.

Furthermore, we have experienced no leaking or valve failures in both Ref. 6 and this work. Therefore, the fluid manipulation repeatability of the device presented in this manuscript is expected to be able to handle the envisioned *in vivo* tasks.

Additionally, although there are many different possible applications for this technology, we have chosen to demonstrate the *bone* tissue engineering use case as a proof of concept. Specifically, we developed a device that could potentially be implanted in an 8 mm diameter critical size defect in a rat's skull.[5,7] This is a "gold standard" model for testing engineered bone tissue scaffolds in living animals. Likewise, we chose to work with the well-

TABLE I. Scaling capacity of the multiplexer plumbing assuming a 4 × 4 addressable implant. Note: The design for the addressable implant optimized for a fixed number of 22 multiplexed channels will be used for the implant payload channels, the implant control channels, and the sample chip vacuum channels. Also, note that the number of control lines can only be an even number for a combinatorial multiplexer.

No. of Control Lines	Total possible multiplexed channels	No. of remaining possible multiplexed channels	Remaining possible multiplexed junctions (n)	Total possible SAAC microwells (4 × n array)	Total possible time points and/or signals
8	70	46	23	92	5 (11)
10	252	228	114	456	28
12	924	900	450	1 800	112
14	3 432	2 410	1205	6 820	426
16	12 870	12 848	6424	25 696	1606

characterized PLLA biomaterial, although in principle, any kind of implant could be potentially analyzed by our device (just as long as it is not too soft to be supported by a bolt, and its structural integrity can handle the slight pressure changes in the device).

Finally, although we have shown that the technology works in a laboratory setting, with water carrying food dyes as simulated bodily fluids, much work remains to be done in terms of implementation of the technology in an actual *in vivo* setting, with analysis of cell secretions (instead of relying on histology of the explanted sample). Therefore, Secs. III A–III C go into deeper details as to what remains to be accomplished.

A. Accounting for external tubing and wiring during the implantation of the microfluidics device into a living animal

Much more ambitious implantations of artificial devices into the heads of living animals have been done before. Specifically, in microdialysis experiments, externally wired probes continuously collect chemicals (e.g., neurotransmitters, peptides, electrolytes) from the brains of the test subjects, who then remain attached to the external pumping and analysis hardware for weeks at a time.[10–13] Therefore, it is reasonable to expect that our device too can be tolerated by the rats, given that it would not invade as deeply into their craniums.

Furthermore, useful knowledge should be borrowed from these previous works to avoid the potential pitfalls that have already been overcome by them. For example, although the implantation protocols for the critical cranial defect's surgical procedures are well established,[24] the conventional tissue engineering scaffolds are typically implanted in their *entirety,* below the periosteum. However, in the cases of both, our device and the microdialysis probes, external hardware components, such as wiring and tubing, protrude from the animal's head permanently after the surgery [as in Fig. 1(b)]. Therefore, the calvarial defect protocol should be *modified* in order to account for the implanted microfluidics device being connected to the external hardware components. As a possibility, the entire device assembly could be glued to the animal's skull using dental acrylic, as was done in the microdialysis studies. After that, the periosteum subcutaneous tissue would be placed over the resin, to improve adherence and sutured using 4-0 vicryl®. The skin would then be similarly sutured with 3-0 silk. Finally, the tubing protruding from the top of the head should be glued in place using the dental acrylic.

B. Assessing the biomaterial implant's performance using *ex vivo* ELISA assays of the *in vivo* fluid samples

Given that most of the probings will be secretions by the cells (and not the cells themselves), histology of the samples collected from the *in vivo* environment is implausible. Luckily, sandwich ELISA assays present the perfect opportunity for analyzing the biomaterial implant's performance *in vivo*. Specifically, they can be used to quantify the tissue in-growth from the host's body based on the following common bone-specific markers:

1. DIFFERENTIATION

Osteogenic commitment of stem cells (responsible for new tissue synthesis) can be monitored via sandwich ELISA assays that analyze the collected liquid for the secretion of (BMP-2)[25] and Osteocalcin (OC)[26]—bone-specific proteins synthesized by osteoblast bone cells.

2. Extracellular matrix (ECM) synthesis

Bone-specific alkaline phosphatase (BAP)[27,28] and procollagen type I carboxy-terminal propeptide (PICP) (an indicator of bone type I Collagen)[29] ELISA can be used to monitor the synthesis of the "hard" (i.e., calcified) and "Soft" (primarily Collagen I) ECM formation, respectively.

Table II is summaries the four proposed ELISA signal readouts for the engineered bone implant analysis application.

However, given that, to the best of our knowledge, the ELISA assays have not been used to analyze *in vivo* bone formation in real time (as does our technology). So, its results should be sufficiently validated prior to implementation in a clinical testing. This can be done through a variety of ways. For example, by comparing the ELISA results to literature data that quantify bone regeneration in PLLA implants via conventional microscopy assays (e.g., ALP, Alizarin Red, proteoglycans, etc.).[30–37] Or, this can be done by explanting the scaffolds at the very end of the experiment (i.e., when the animal is euthanized), followed by conventional staining assays/histology performed on the retrieved samples to check for a confirmation of the bone formation and for an absence of collagen signals. Although not real-time, these measurements would provide more confidence to device readouts using more traditional approaches.

C. Miniaturizing supporting hardware to make the device completely wearable by the animal

As mentioned in Sec. III A, having a live animal being permanently connected to external hardware can present a problem with it attempting to detach itself and in the process dislodging and/or damaging the implanted device. Hence, in the ideal case scenario, the external hardware, such as those responsible for operating the device, should be miniaturized so that it can be fitted into a "backpack" worn by the rodent (see Fig. 11-left). For example, the programmable logic controller/house air setup currently operating our device[20,38,39] can be substituted with something like the iPRECIO® SMP-200 programmable microinfusion pump, which was designed specifically for rats with the following characteristics: (1) 6 months

TABLE II. Summary of possible sandwich ELISA assays for bone regeneration analysis.

Monitored tissue regeneration	Secretion assays
Differentiation to osteoblast lineage	BMP-2[25]
	OC[26]
Bone extracellular matrix (ECM)	Hard ECM: BAP[27,28]
	Soft ECM: PICP[29]

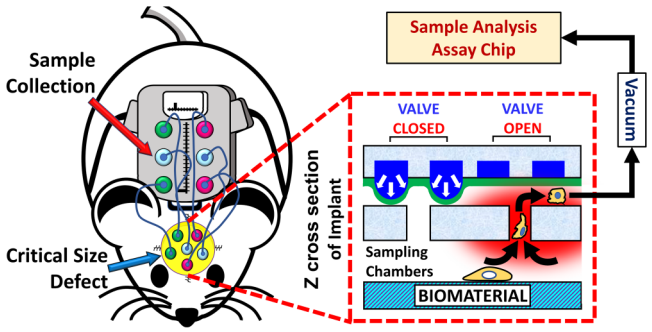

FIG. 11. Overview of the miniaturized version of the conceptualized technology. (Left) A lab rodent with a biomaterial-testing device implanted into a critical sized defect in its skull (yellow). All the electronics pressurizing and driving the device as well as the supporting microfluidics chips that do the multiplexing and the analysis are fitted into a "backpack" worn by the rodent. (Right) Side view of the microfluidics device that uses the addressable ports to probe cells and fluids at targeted locations within the implant. When the blue valve is inflated, the port is closed off; but when the valve is not actuated, negative pressure is used to collect a micro- "biopsy" and send it off for *ex situ* analysis.

battery life; (2) 147 g weight; (3) 12 × 6.7 × 3.5 cm size; (4) wireless communications. Additionally, the external solenoid valves in our setup can be replaced with VHS Series miniature solenoid valves made by The Lee Company. They were designed for applications requiring precise dispense volumes in the microliter to nanoliter range and have a weight of just 1.8 g and a size of 2 cm length × 0.5 cm diameter.

Of course, a miniature power source, like a watch battery, should be included into the "backpack." Additionally, the readings of the ELISA measurements could be done on the SAAC *automatically*. This can be accomplished based on O_2 concentration generated from enzymatic digestion of H_2O_2 substrate (pre-loaded into the microwells).[40] Once the gas is produced, it would displace a dye into a microfluidics readout channel with markings that correspond to different pressures (similar to how temperature is read from the gradations of a mercury thermometer). These values will then be indicative of the bone generation markers in the implant at each time of the probes' collections. Furthermore, the reading can be done by using a small LED light + sensor combination and possibly even transmitted wirelessly using a miniature Wi-Fi module. The latter could also be used for sending command signals to the system remotely.

IV. CONCLUSIONS

In this manuscript, we have presented a novel microfluidic platform potentially capable of performing nondisruptive fluid manipulations within the spatial constraints of an 8 mm diameter critical calvarial defect. The intent of this work is to lay the foundation for ultimately implanting the device into the skull of a rat and obtaining real-time *in vivo* readouts of bone in-growth signals that can be compared against existing literature and end-point explantation analysis. The device would potentially be able to sample up to 16 different locations above the biomaterial's surface at a time, and the collected fluids would then be flown out of it continuously for *ex vivo* analysis (thereby overcoming the need for sacrificial explantation of the scaffold). The external microfluidic pluming supporting the storage and analysis of the samples can be scaled up indefinitely to handle additional timepoints and biological signal measurements. Furthermore, sandwich ELISA tests are proposed for quantifying the bone regeneration occurring in the implant based on the collected fluid samples. Future improvements to the technology include modifying the implantation protocols to fixate the device in the animal's head; and miniaturizing the external hardware to make the entire system fully wearable by the host. Although the proof-of-concept application has focused on engineered bone implants, in principle, the technology is potentially versatile enough for other *in vivo* sampling applications. Thus, the successful outcomes of its advancement should benefit companies developing, testing, and producing vaccines and drugs, by accelerating the translation of advanced cell culturing technologies to the clinical market. Moreover, the nondestructive monitoring of the *in vivo* environment is expected to lower animal experiment costs and provide data-gathering continuity superior to the conventional destructive analysis. Last, the reduction of the sacrifices stemming from the use of this technology should make future animal experiments more ethical.

ACKNOWLEDGMENTS

Research reported in this publication was supported by the National Center for Advancing Translational Sciences (NCATS), a component of the National Institute of Health (NIH) under Award No. UL1TR003017. The content is solely the responsibility of the authors and does not represent the official views of the National Institutes of Health.

AUTHOR DECLARATIONS

Conflict of Interest

Anh Tong and Roman Voronov have a Provisional U.S. patent Application No. 63/425,168 submitted on November 14, 2022.

Ethics Approval

This article does not contain any studies with human participants or animals performed by any of the authors.

Author Contributions

M.N. and A.T. are the first two authors who contributed equally to the manuscript.

Minh Nguyen: Formal analysis (equal); Methodology (equal); Validation (equal); Visualization (equal); Writing – review & editing (equal). **Anh Tong:** Conceptualization (equal); Data curation (equal); Formal analysis (equal); Methodology (equal); Project administration (equal); Software (equal); Validation (equal); Visualization (equal); Writing – original draft (equal). **Mark Volosov:** Software (equal); Validation (equal); Writing – review & editing (equal). **Shreya Madhavarapu:** Methodology (equal). **Joseph Freeman:** Funding acquisition (equal); Investigation

(equal); Project administration (equal); Resources (equal); Supervision (equal); Writing – review & editing (equal). **Roman Voronov:** Conceptualization (equal); Data curation (equal); Formal analysis (equal); Funding acquisition (equal); Investigation (equal); Project administration (equal); Resources (equal); Supervision (equal); Writing – original draft (equal); Writing – review & editing (equal).

DATA AVAILABILITY

The data that support the findings of this study are available from the corresponding author upon reasonable request.

REFERENCES

[1]D. G. Brown, H. J. Wobst, A. Kapoor, L. A. Kenna, and N. Southall, Nat. Rev. Drug Discovery **21**, 793 (2021). .
[2]O. J. Wouters, M. McKee, and J. Luyten, Jama **323**, 844–853 (2020).
[3]A. Mullard, Nat. Rev. Drug Discovery **15**, 447–448 (2016).
[4]M. J. Webber, O. F. Khan, S. A. Sydlik, B. C. Tang, and R. Langer, Ann. Biomed. Eng. **43**, 641–656 (2015).
[5]P. P. Spicer, J. D. Kretlow, S. Young, J. A. Jansen, F. K. Kasper, and A. G. Mikos, Nat. Protoc. **7**, 1918–1929 (2012).
[6]A. Tong, Q. L. Pham, V. Shah, A. Naik, P. Abatemarco, and R. Voronov, ACS Biomater. Sci. Eng. **6**, 1809–1820 (2020).
[7]G. M. Cooper, M. P. Mooney, A. K. Gosain, P. G. Campbell, J. E. Losee, and J. Huard, Plast. Reconstr. Surg. **125**, 1685 (2010).
[8]M. M. Stevens, Mater. Today **11**, 18–25 (2008).
[9]A. Kashirina, Y. Yao, Y. Liu, and J. Leng, Biomater. Sci. **7**, 3961–3983 (2019).
[10]E. L. Varner, C. L. Leong, A. Jaquins-Gerstl, K. M. Nesbitt, M. G. Boutelle, and A. C. Michael, ACS Chem. Neurosci. **8**, 1779–1788 (2017).
[11]J. Teixidor, S. Novello, D. Ortiz, L. Menin, H. A. Lashuel, A. Bertsch, and P. Renaud, bioRxiv (2022).
[12]Y. Da, S. Luo, and Y. Tian, ACS Appl. Mater. Interfaces **15**, 138–157 (2022).
[13]A. Miled, H. Landari, M. Boukadoum, and Y. Messaddeq, *Handbook of Biochips* (Springer, 2022), pp. 731–742.
[14]H. Takehara, A. Nagaoka, J. Noguchi, T. Akagi, H. Kasai, and T. Ichiki, Sci. Rep. **4**, 6721 (2014).
[15]K. Brower, A. K. White, and P. M. Fordyce, J. Visualized Exp. **119**, e55276 (2017).
[16]Q. L. Pham, N. A. N. Tong, A. Mathew, S. Basuray, and R. S. Voronov, Biomicrofluidics **12**, 044119 (2018).
[17]Y. Gao, J. Tian, J. Wu, W. Cao, B. Zhou, R. Shen, and W. Wen, RSC Adv. **6**, 101760–101769 (2016).
[18]X. Li, Z. T. Yu, D. Geraldo, S. Weng, N. Alve, W. Dun, A. Kini, K. Patel, R. Shu, F. Zhang, G. Li, Q. Jin, and J. Fu, Rev. Sci. Instrum. **86**, 075008 (2015).
[19]H.-Y. Wang, N. Bao, and C. Lu, Biosens. Bioelectron. **24**, 613–617 (2008).
[20]K. Brower, R. Puccinelli, C. J. Markin, T. C. Shimko, S. A. Longwell, B. Cruz, R. Gomez-Sjoberg, and P. M. Fordyce, HardwareX **3**, 117–134 (2018).
[21]J. Melin and S. R. Quake, Annu. Rev. Biophys. Biomol. Struct. **36**, 213–231 (2007).
[22]M. Sesen and C. J. Rowlands, Microsyst. Nanoeng. **7**, 48 (2021).
[23]J. Briones, W. Espulgar, S. Koyama, H. Takamatsu, E. Tamiya, and M. Saito, Sci. Rep. **11**, 1–12 (2021).
[24]R. Khorramirouz, J. L. Go, C. Noble, S. Jana, E. Maxson, A. Lerman, and M. D. Young, Acta Histochem. **120**, 282–291 (2018).
[25]Y. Zhang, Z. Gazit, G. Pelled, D. Gazit, and G. Vunjak-Novakovic, Integr. Biol. **3**, 39–47 (2010).
[26]A. Nakamura, Y. Dohi, M. Akahane, H. Ohgushi, H. Nakajima, H. Funaoka, and Y. Takakura, Tissue Eng. Part C: Methods **15**, 169–180 (2009).
[27]J. M. Roudsari and S. Mahjoub, Caspian J. Intern. Med. **3**, 478 (2012).
[28]E. E. Golub and K. Boesze-Battaglia, Curr. Opin. Orthop. **18**, 444–448 (2007).
[29]W.-Y. Seo, J.-H. Kim, D.-S. Baek, S.-J. Kim, S. Kang, W. S. Yang, J.-A. Song, M.-S. Lee, S. Kim, and Y.-S. Kim, Sci. Rep. **7**, 15946 (2017).
[30]F. Gang, W. Ye, C. Ma, W. Wang, Y. Xiao, C. Liu, and X. Sun, Materials **15**, 4280 (2022).
[31]C.-H. Cheng, M.-Y. Shie, Y.-H. Lai, N.-P. Foo, M.-J. Lee, and C.-H. Yao, Polymers **13**, 3731 (2021).
[32]M. Bahraminasab, A. Talebi, N. Doostmohammadi, S. Arab, A. Ghanbari, and S. Zarbakhsh, J. Orthop. Surg. Res. **17**, 1–17 (2022).
[33]L. Zhou, R. Quan, J. Yang, and H. Xu, Ann. Transl. Med. **9**, 1–17 (2021).
[34]T. Zheng, Y. Yu, Y. Pang, D. Zhang, Y. Wang, H. Zhao, X. Zhang, H. Leng, X. Yang, and Q. Cai, Compos. Part B: Eng. **234**, 109734 (2022).
[35]S. Tanodekaew, S. Channasanon, P. Kaewkong, and P. Uppanan, Proc. Eng. **59**, 144–149 (2013).
[36]Y. Liu, C. Xu, Y. Gu, X. Shen, Y. Zhang, B. Li, and L. Chen, RSC Adv. **9**, 11722–11736 (2019).
[37]X. Zhang, J.-L. Chen, F. Xing, and X. Duan, J. Mater. Sci.: Mater. Med. **33**, 71 (2022).
[38]R. Gomez-Sjoberg, A. A. Leyrat, D. M. Pirone, C. S. Chen, and S. R. Quake, Anal. Chem. **79**, 8557–8563 (2007).
[39]R. Gómez-Sjöberg, see https://sites.google.com/site/rafaelsmicrofluidicspage/home for Rafael's microfluidics page.
[40]D. Liu, X. Li, J. Zhou, S. Liu, T. Tian, Y. Song, Z. Zhu, L. Zhou, T. Ji, and C. Yang, Biosens. Bioelectron. **96**, 332–338 (2017).